World Academy of Science, Engineering and Technology
International Journal of Aerospace and Mechanical Engineering
Vol:16, No:10, 2022

Aerodynamic Design of Three-Dimensional Bellmouth for Low-Speed Open-Circuit Wind Tunnel

Harshavardhan Reddy, Balaji Subramanian

***Abstract*—**A systematic parametric study to find the optimum Bellmouth profile by relating geometric and performance parameters to satisfy a set of specifications is reported. A careful aerodynamic design of Bellmouth intake is critical to properly direct the flow with minimal losses and maximal flow uniformity into the honeycomb located inside the settling chamber of an indraft wind tunnel, thus improving the efficiency of the entire unit. Design charts for elliptically profiled Bellmouth's with two different contraction ratios (9 and 18) and three different test section speeds (25 m/s, 50 m/s, and 75 m/s) were presented. A significant performance improvement - especially in the coefficient of discharge and in the flow angularity and boundary layer thickness at the honeycomb inlet - was observed when an entry corner radius (r/D = 0.08) was added to the Bellmouth profile. The nonuniformity at the honeycomb inlet drops by about three times (~1% to 0.3%) when moving from square to regular octagonal cross-section. An octagonal cross-sectioned Bellmouth intake with L/d = 0.55, D/d = 1.625, and r/D = 0.08 met all the four target performance specifications and is proposed as the best choice for a low-speed wind tunnel.

***Keywords*—**Bellmouth intake, low-speed wind tunnel, coefficient of discharge, nonuniformity, flow angularity, boundary layer thickness, CFD, aerodynamics.

I. Introduction

A Bellmouth intake is provided at the inlet of a settling chamber (or plenum) to facilitate the suction of outside ambient air into a conventional open-circuit wind tunnel. The purpose of a Bellmouth intake is to align and accelerate the flow efficiently towards the constant area settling chamber duct, in the process delivering 'good quality flow' to the first row of flow conditioning devices, namely, the honeycomb located inside the settling chamber. Here, the term 'good quality flow' is quantified and benchmarked using the performance parameters: flow nonuniformity, flow angularity, boundary layer thickness, and wall pressure coefficient. There are many possibilities for shaping a Bellmouth profile [1]-[4]. Any smooth converging (convex) curve swept along the inlet perimeter of a settling chamber duct is expected to reduce intake losses and improve the flow quality at the Bellmouth exit.

Before discussing the role of a Bellmouth intake on wind tunnel's performance, a brief overview of the general-purpose low-speed wind tunnel facilities operating worldwide is provided. The general-purpose wind tunnels are classified based on their configuration into open-circuit and closed-circuit type facilities. In the open-circuit type, air particles at the tunnel's centerline follow a straight path from the Bellmouth entrance passing through the settling chamber and a contraction nozzle to reach the test section. The air particles then continue their journey along the same track, passing through a diffuser mounted with an axial fan at its exit before exhausting back to the ambient atmosphere. In closed-circuit type wind tunnels, a fixed mass of air keeps recirculating continuously through the loop, and there is little or no interaction with the outside ambient atmosphere. Bellmouth intakes are present only in open-circuit type wind tunnels. Open-circuit wind tunnels come in various shapes and forms, ranging from tabletop demonstration tunnels to the largest governmental and industrial facilities operating worldwide. The overall length of these wind tunnels is at least one order of magnitude larger than its corresponding test section dimension. These general-purpose facilities are indispensable tools for aerodynamic research and technological development in the energy, aerospace, and automotive sectors. A detailed description of general-purpose wind tunnels is provided in [5].

There is already a wealth of literature [3]-[14] directed at helping designers improve the efficiency and reduce the cost of all other open-circuit wind tunnel components, namely, nozzle [15]-[21], diffuser [22]-[27], fan [3], [6], [7], [12], [28], and the various other flow conditioning devices [29]-[38] present inside the settling chamber. The flow conditioning devices - honeycomb and damping screens - are always placed in the settling chamber to reduce the overall wind tunnel power requirements [5]. These studies clearly outline the optimum design approach involved in sizing the aforementioned components. Suppose a steady, low turbulence flow is desired in the test section. In that case, a carefully designed large Contraction Ratio (CR) nozzle along with a proper selection of Bellmouth intake is employed in conjunction with the right choice of honeycomb and a larger than usual number of screens to damp out turbulence. Damping screens, in particular, are known to play an essential role in obtaining low turbulence levels in the test section [5], [14], [29]. If any wind tunnel component is not designed correctly, then it will affect the performances of all the other upstream and downstream subsystems. This results in poor test section flow quality and a reduction in the overall wind tunnel efficiency. Though much care is needed in designing an optimum Bellmouth intake for a low turbulence wind tunnel, the guidance available to designers is scattered [1]-[3], [12], [39] and not properly documented in the open literature.

During regular operations, the steady airflow inside an

Harshavardhan Reddy and Balaji Subramanian∗ are with Department of Mechanical Engineering, Indian Institute of Technology Tirupati, Andhra Pradesh, India (∗e-mail: balaji@iittp.ac.in).

indraft open-circuit wind tunnel is driven by an axial fan placed at the exit end of a diffuser. This unit requires an efficient means to ingest the ambient atmospheric air and guide it downstream into the settling chamber without any separation. A Bellmouth intake serves this purpose perfectly. If the ambient air is simply ingested without a Bellmouth intake into the settling chamber, the entry pressure loss coefficient tends towards 0.5 [40]. The stream tube at the settling chamber inlet contracts initially and then expands downstream to fill the entire duct, forming vena contracta and large-scale swirl eddies in the process, which contributes to losses, nonuniformity, and unsteadiness. For large CR's (say, nine or above), the maximum expected flow speed in the settling chamber is about one order of magnitude smaller than their corresponding values in the test section. The entry losses will be less severe at these low flow speeds even if the settling chamber inlet does not have a Bellmouth attached to it. However, the absence of a Bellmouth intake results in poor flow quality at the honeycomb inlet, increasing the total pressure losses across the honeycomb and in all the other flow conditioning devices located downstream, thus producing a cascading effect on the wind tunnel's performance. A proper Bellmouth design significantly influences the overall performance of a wind tunnel, while an inept Bellmouth design can cause problems and degrade its performance.

Bellmouth, like nozzle, can be effectively isolated from the performance of the remainder of the tunnel components and separately analyzed [3], [5], [41]. The problem is that there is an infinite number of possible Bellmouth intake profiles. Researchers already assessed several potential candidates in the past [1], [2] systematically evaluated and benchmarked their performances to find the optimum profile shape. Even simple Bellmouth profiles like a quarter or a half-circle, with a diameter half the effective duct diameter to which it is connected, were reported to produce significant performance improvement [1], [2]. Other Bellmouth profiles evaluated include a 3-circles profile, an airfoil profile, and an elliptic profile. A good choice of Bellmouth profile optimized for a particular wind tunnel geometry and flow condition can yield significant gains in performance. All researchers unanimously recommend [1]-[12] employing an elliptically profiled Bellmouth in low-speed, indraft wind tunnels because it produces a substantial improvement in the Coefficient of discharge (Cd) and the quality of flow delivered to the honeycomb. One-quarter of an ellipse is considered the best choice for a Bellmouth intake profile (shown in Fig. 1). Incidentally, an elliptical profile is also employed in the aircraft engine intakes [23], [39]. It is worth noting here that only two geometrical parameters (semi-major and semi-minor axis) are needed to define an elliptical profile completely. Tiwari et al. [1] reported that an elliptical profile resulted in the shortest Bellmouth with minimum boundary layer thickness.

Bellmouth intakes find application in various areas [42]-[46]. For example, water is drawn from a reservoir through a Bellmouth-shaped intake in hydroelectric power plants and fed to the turbine. Bellmouth's are always employed at intakes of reciprocating and gas turbine engines, where they ensure a proper supply of ambient air under all operating conditions. Smoke flow visualization studies employ a large CR indraft subsonic wind tunnel with a Bellmouth intake. In general, a Bellmouth-shaped intake is widely used [13], [26], [47] when fluid needs to be efficiently drawn from a reservoir through a duct, as it ensures maximum fluid flow with minimum losses. A Bellmouth intake design is predominantly guided by two principles: minimizing cost and maximizing efficiency. In the case of wind tunnels, one more principle guides a Bellmouth intake design, which is the exit flow quality as it dictates the position of and losses incurred in the honeycomb downstream. The focus in this manuscript is only on Bellmouth design for low-speed wind tunnels. Fifty years ago, Mehta [12] summed up the state of Bellmouth intake design for wind tunnels in the following way "A Bellmouth presents a fairly uniform flow to the blower inlet. The inlet Bellmouth can be shaped into a quarter of an ellipse, with its major semi-axis equal to the equivalent inlet diameter and its minor semi-axis equal to three-eighths of the major axis". Since then, we have come a long way [3], [9], [14].

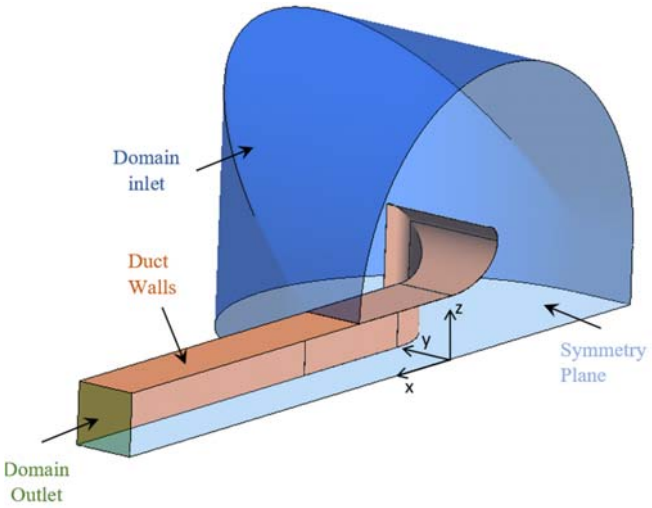

Fig. 1 Computational domain: one-quarter of the full Bellmouth geometry with the axis located at Bellmouth exit: A constant cross-sectional area duct of length four hydraulic exit diameters is provided downstream of the Bellmouth exit [2]

Assuming no flow separation at the entry tip edge region, a laminar boundary layer forms from the inlet of a Bellmouth, starts to grow over its walls along the flow direction and then transitions to a turbulent state downstream. As the ambient air enters and accelerates through a Bellmouth, the fluid particles near the Bellmouth wall 'locally' encounter large convex curvature that produces more acceleration in these particles than their counterparts around the centerline. This accelerating flow field establishes a favorable pressure gradient inside the Bellmouth. It is a natural tendency of fluid following a convex curvature to over speed [41], resulting in a non-uniform velocity distribution at the Bellmouth exit plane. A non-uniform flow at the Bellmouth exit influences the position and performance of the honeycomb in the settling chamber.

The static pressure is essentially constant [41] within the attached boundary layer. Thus, the static pressure variation on

Bellmouth walls provides insight into static pressure distribution in the freestream just outside the boundary layer. As the Bellmouth exit flow enters into a constant area settling chamber duct, the fluid particles near the wall must decelerate, ensuing in a region of adverse pressure gradient and creating a possibility for boundary layer separation. The magnitude of the adverse pressure gradient is reduced by going for a longer Bellmouth, but this increases the boundary layer thickness at the Bellmouth exit and increases the tunnel's size and cost. As the average flow speeds at Bellmouth exit are typically small for large CR's, these effects are much more critical in the case of a contraction nozzle than with Bellmouth.

There is a high risk of inlet flow separation in Bellmouth intakes. A flow separation either at the inlet or near the exit of a Bellmouth can result in unsteady free shear layers and recirculating regions, effectively altering the intake geometry and affecting the performance of all downstream components. The inlet flow separation can be intermittent, resulting in significant unsteadiness in the test section. Avoiding these separation swirl irregularities is contingent on correctly designing a Bellmouth intake. This work aims to understand all factors influencing an indoor mounted Bellmouth's performance and develop suitable intake design charts for low-speed, subsonic wind tunnels. If the inlet of a Bellmouth is located outdoors, it can be influenced by wind, rain, dust, etc., in its vicinity, and such intakes must be designed to cope with various upstream ambient conditions.

Some earlier works [48], [49] focused on finding the right Bellmouth intake profile using potential flow analysis for two-dimensional or axisymmetric cases. However, the actual flow inside a Bellmouth is three-dimensional, with complex turbulence structures, and the flow quality downstream of a Bellmouth is determined primarily by viscous effects. This work aims to apply the existing tools and techniques to perform a comprehensive three-dimensional analysis of Bellmouth flows considering viscous effects. The goal is to develop rational design charts to enhance the understanding of elliptically profiled Bellmouth's employed in low-speed wind tunnels. This goal is realized by systematically studying the parameters influencing a Bellmouth's performance.

The objective is to design the smallest sized Bellmouth for a low-speed wind tunnel having large CR's (> 9) and with test section flow speeds ranging from 25 m/s to 75 m/s, meeting the following criteria (or specifications).

1. Coefficient of Discharge, $C_d > 0.95$ (this at all three test section speeds)
2. Maximum pitch (θ_{max}) and yaw (Ψ_{max}) angles on the vertical and horizontal symmetry planes at the honeycomb inlet < 1° at a test section speed of 50 m/s.
3. Nonuniformity ($\tilde{u}$) at the honeycomb inlet < 1% (there is no separate criteria for C_{pe}) at a test section speed of 50 m/s.
4. Non-dimensional boundary layer thickness ($\frac{\delta}{d/2}$) on the vertical and horizontal symmetry planes at the honeycomb inlet < 5% at a test section speed of 50 m/s.

An optimized Bellmouth design must satisfy all these four performance parameter specifications. The improvement in performance gained by adding a quarter circle with an entry corner radius of 'r' to a Bellmouth profile will be analyzed and quantified. The resulting Bellmouth design must cost less and occupy less space. It is also important to reduce the settling chamber length by placing the honeycomb as close to the Bellmouth exit as possible but still meeting the above performance parameter specifications. The optimum location of the honeycomb from the Bellmouth exit will be found as a part of this study. Finally, though the Bellmouth and settling chamber were assumed to have a square cross-section, a considerable improvement in flow nonuniformity at the honeycomb inlet was observed when converting a square into a regular octagonal cross-section, as reported in this manuscript. The impact of square and regular octagonal cross-sectional geometry on a Bellmouth performance will be presented.

II. Computational Setup

Design charts for Bellmouth's with pressure ratios less than 1.01 - at two different CR's and three different test section flow speeds (i.e., Re_d) at each CR - are developed using viscous, incompressible flow analysis to aid in finding the optimum Bellmouth geometry for a low-speed wind tunnel. Commercial CFD tools, like Ansys [50], have become fast, accurate, and reliable resources for solving engineering problems. The simulations are executed in the Ansys Fluent [51], [52] to understand the turbulent flow behavior in a Bellmouth intake. An integrated package in the Ansys workbench, ICEM, was employed for meshing. At the same time, the CFD simulations and postprocessing were performed in the Fluent module, which uses a finite volume-based solver. As the underlying physical phenomena are complex and non-linear, these turbulent flow simulations were carried out by solving the Reynolds Averaged Navier Stokes (RANS) equations coupled with the Shear Stress Transport (SST) κ-ω turbulence model [53] using a second-order scheme. The κ–ω SST turbulence model [53] is based on two transport equations (one for the turbulent kinetic energy κ, and the other for specific turbulent dissipation rate ω) and is chosen here because it is known to be very accurate in solving the flow field near-wall regions [54], [55].

The RANS based partial differential equations for incompressible and steady flow are:

$$\frac{\partial}{\partial x_i}(\overline{u_\iota}) = 0 \tag{1}$$

$$\rho\,\overline{u_\jmath}\frac{\partial}{\partial x_j}(\overline{u_\iota}) = -\frac{\partial \bar{p}}{\partial x_i} + \mu\frac{\partial}{\partial x_j}\left[\left(\frac{\partial \overline{u_\iota}}{\partial x_j}\right)\right] - \rho\frac{\partial}{\partial x_j}(\overline{u_\iota' u_j'}) \tag{2}$$

The Reynolds stress term $\rho\overline{u_\iota' u_j'}$ is resolved according to the chosen turbulence model. An eddy viscosity-based turbulence model is chosen here to provide closure for the RANS equations. In the RANS approach, the turbulent fluctuations are time averaged. Hence, the mean flow properties could be accurately predicted using this approach. The numerical investigation presented here assumes the flow to be steady, incompressible, and isothermal.

The computational domain is shown in Fig. 1. The air is sucked into a Bellmouth from the ambient atmosphere, and it is important to correctly capture the inlet tip edge flow as it affects a Bellmouth's performance [1], [2]. Thus, an outer region in the immediate vicinity of a Bellmouth intake is included in the computational domain. The computational domain inlet is located at a minimum distance of two hydraulic diameters (i.e., 2xD, Ref. Fig. 2) from the Bellmouth inlet in all directions. The domain outlet is located on a constant cross-sectional area duct at a distance of four hydraulic diameters (i.e., 4xd, Ref. Fig. 2) from the Bellmouth exit [2]. The actual flow inside a square cross-sectional Bellmouth will be three-dimensional, with complex turbulent structures [41], [56]. A three-dimensional domain captures the influence of the inlet tip edge corner and duct corner on the resulting Bellmouth flow field. Computational investigations with three-dimensional CFD simulations are valuable but remain very time-consuming. At steady state, the flow field is assumed to be symmetric about a horizontal and a vertical plane passing through the Bellmouth centerline. Thus, only a quarter of the whole domain was selected for simulations to understand the flow physics of various Bellmouth geometries, Fig. 1. This simplification helps to minimize the computational efforts involved with each simulation. Though only one-quarter of the whole geometry was employed, each simulation still took ~3 hours to complete on a High-Performance Computing (HPC) cluster with 64 processors. A total of ~300 such simulations were performed as a part of the study reported here. The design charts reported in this manuscript were prepared using the computational domain shown in Fig. 1. A few simulations were executed with the final optimized Bellmouth design but using the whole geometry to check the consistency of the results presented here.

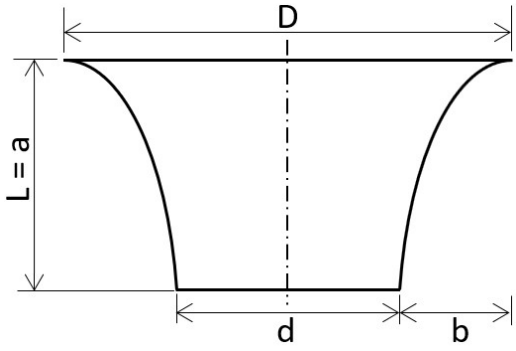

Fig. 2 Bellmouth profile

The geometry was modelled in CREO with a tolerance of 10^{-6} m and imported into the Ansys workbench. A high-quality unstructured tetrahedral mesh, with near-wall regions refined using 39 prism layers, was generated in ICEM to facilitate the study of turbulent boundary layer growth on bellmouth duct walls. Enhanced wall treatment requires the first cell centroid near the wall to be located within the viscous sublayer. To get y+ < 1 on all duct walls, the height of the first prism layer is maintained at 50 microns everywhere, which helps resolve the viscous sublayer directly (see Fig. 4). A growth rate of 1.2 is specified in the inflation region.

A Dirichlet type boundary condition is prescribed at the inlet and outlet of the computational domain. The total pressure value at the domain inlet is set to 0 Pa (gauge), while the mass flow rate calculated using test section flow speeds is specified directly at the domain outlet. A smooth, no-slip boundary condition is assumed on all the duct walls. The turbulence inflow into the domain is assumed as isotropic, with turbulence intensity of 2% and a length scale of 5 mm taken for all simulations. A thorough mesh sensitivity study was performed to ascertain that the results presented here are independent of mesh resolution. Convergence is monitored by tracking the scaled residuals in each iteration, which measures the overall conservation of flow properties. The convergence criterion (relative error of the calculated parameters) specified in the solver is 10^{-6}.

A parametric study was performed to understand the impact of domain inlet turbulence intensity and length scales on all Bellmouth performance parameters. This sensitivity study was performed at a test section flow speed of 50 m/s with the final optimized Bellmouth design configuration (i.e., L/d = 0.55, D/d = 1.625 and r/D = 0.08). Three length scales (1 mm, 5 mm, and 50 mm) and three turbulence intensities (1%, 2%, and 5%) were considered in this study. For the range of turbulence intensities and length scales considered here, it was found that the changes in Bellmouth performance parameters were negligibly small (< 0.1%).

III. Elliptically Profiled Bellmouth

Bellmouth in this manuscript refers to an elliptically profiled Bellmouth intake unless otherwise stated. A typical Bellmouth profile is shown in Fig. 2. If the axial length of a Bellmouth is 'L', and the hydraulic diameters at Bellmouth inlet and exit are 'D' and 'd', respectively, then two non-dimensional geometric parameters, 'L/d' and 'D/d', can be constructed using these dimensions. These non-dimensional parameters characterize a Bellmouth geometry as the ratios 'L/d' and 'D/d' help determine the semi-major and semi-minor axes of the elliptical profile, respectively.

Presently wind tunnel designers rely on the ESDU datasheet 80037 [39] to correctly size their Bellmouth's [3]. However, this data sheet is for Bellmouth's employed in the aircraft engine intakes at various subsonic speeds. It recommends choosing an elliptically profiled Bellmouth with an axis ratio between 2 to 5, where this ratio is defined as the ratio of an ellipse's semi-major and semi-minor axes. A small axis ratio is preferred as it is desirable to minimize the length occupied by a Bellmouth. For example, Johl [3] noted "To ease construction, an elliptic Bellmouth with a semi-major axis of 600 mm and semi-minor axis of 275 mm was chosen, resulting in an axis ratio of 2.2". However, both numbers in this axis ratio are not known, and the only known dimension available to the designers is the hydraulic diameter of the settling chamber 'd'. Thus, the sizing of the semi-major and semi-minor axes is performed as a part of the Bellmouth design process. The axis ratio values considered in this study range from 0.667 to 18.

IV. IIT Tirupati Wind Tunnel

The optimal Bellmouth design proposed here is for a large low-speed wind tunnel under development at Indian Institute of Technology (IIT) Tirupati, India. The state-of-the-art facility will have a cuboidal-shaped test section with dimensions of 2 m (L) × 0.87 m (W) × 0.6 m (H), and with a maximum test section speed of 60-70 m/s. The final goal is to build India's lowest turbulence open-circuit wind tunnel test facility at IIT Tirupati. The flow, in this case, is driven by an axial pressure gradient established in the circuit by a fan located at the exit end of the wind tunnel. When flow uniformity, steadiness, and turbulence level in the test section are of primary concern, much more emphasis must be given to the design of all wind tunnel components. For example, at higher test section speeds, even the axial fan propeller noise is reported to contribute to turbulence level in the test section [9], [12].

A major portion of the wind tunnel, including its intake, will be located inside a large rooftop enclosure surrounded by walls with louvred windows on all four sides. The aim is to significantly dampen ambient gusts (if any) around the intake and prevent the ingestion of water/solid particles, which might otherwise damage the probes and models located in the working (i.e., test) section. In addition, a safety mesh with a porosity of 0.9 will be placed around the Bellmouth intake, where porosity is a function of wire diameter and weave density [5]. The benefits offered by such a mesh are said to outweigh their pressure loss penalty [3], [5]. A converging nozzle with a CR of 9 or 12 is expected to direct airflow into the test section. The nozzle will have a square cross-section at its inlet and a rectangular cross-section at its outlet, as suggested by Su [18]. Thus, the initial proposal is to go for a Bellmouth with a square cross-section, where the boundary layers in corner regions will be more susceptible to separation than the boundary layers near planes of symmetry [41].

When turbulent flow occurs in a straight square cross-sectional duct, it establishes four pairs of large-scale vortical structures categorized as secondary flows in literature [56]-[58]. The secondary flows can be visualized as nonzero mean flows in transverse planes locked near each of the four corners. It is possible to reduce these secondary flow losses by going for a regular octagonal instead of a square cross-sectional duct [58]. The secondary flow losses may not be critical in the case of Bellmouth design as the mean flow speeds are considerably low in the settling chamber. However, they are expected to significantly impact the performance of the contraction nozzle and the test section [41]. As reported in this manuscript, a regular octagonal-shaped cross-section was found to produce superior quality flow at the Bellmouth exit as well as at the honeycomb inlet.

V. Performance Parameters

Quantitative criteria are needed to guide design decisions. The effectiveness of a Bellmouth intake employed in an indraft wind tunnel is measured using performance parameters like the coefficient of discharge (C_d), flow nonuniformity ($\tilde{u}$), flow angularity ($\pm\theta_{max}$, $\pm\Psi_{max}$), total pressure loss (ΔP_T), wall pressure coefficient (C_{pe}) and the boundary layer thickness (δ). Many of these parameters are interrelated with each other. The most important performance parameter is the C_d, defined as the ratio of actual flow rate to the ideal flow rate at the domain outlet [59], where the domain outlet is located at a distance of four hydraulic diameters (i.e., '4d', check Figs. 1 and 2) downstream from the Bellmouth exit. C_d is computed mathematically [59] using the relation:

$$C_d = \frac{Q_{actual}}{Q_{theoretical}} \tag{3}$$

Traditionally, Bellmouth discharge coefficients are experimentally measured using a steady flow test rig [2]. In the case of compressible flows, C_d will be a function of pressure ratio, where the pressure ratio is defined as the ratio of area-averaged total pressure at the domain inlet to the area-averaged static pressure at the domain outlet. However, for incompressible flows, C_d is a function of the difference between area-averaged total pressure at the domain inlet and the area-averaged static pressure at the domain outlet. More specifically, C_d will depend on the kinematic parameter: Reynolds number calculated based on the Bellmouth exit diameter (Re_d), and the geometrical parameters: L/d, D/d, and ε/d, where ε is the wall surface roughness. The C_d and total pressure loss are strongly correlated with each other (see Fig. 6). The larger the C_d, the lower will be the total pressure drop in a Bellmouth. One of the goals is to increase C_d as much as possible above 0.95 at a test section flow speed of 25 m/s.

$$C_d = f(Re_d, L/d, D/d, \epsilon/d) \tag{4}$$

The magnitude of the velocity vector at any point in the domain is given by,

$$V = \sqrt{u^2 + v^2 + w^2} \tag{5}$$

where the u-, v-, and w-components are along x, y, and z directions, respectively. The criteria associated with flow quality are more complex. Flow nonuniformity at any cross-section measures the relative maximum variation in velocity at that cross-section and is mathematically stated as:

$$\tilde{u}\ (in\ \%) = \frac{V_{max} - V_{min}}{U_{avg}}\ x\ 100 \tag{6}$$

The maximum velocity (V_{max}) at the Bellmouth exit (or at any other cross-section around the Bellmouth exit) occurs near the wall, just outside the boundary layer. This velocity overshoot is nicely captured in CFD simulations. The minimum (V_{min}) velocity occurs at the Bellmouth centerline, and the U_{avg} is the average axial velocity at the domain outlet. The situation desired in the settling chamber is a low-velocity uniform flow as this is where the honeycomb and screens are located, and the low velocity minimizes a wind tunnel's power requirements. The criterion set here for acceptable flow nonuniformity at the honeycomb inlet is $\tilde{u}$ < 1%. An optimized Bellmouth design must satisfy this performance parameter specification.

The pitch angle (θ) at any point on a line, normal to the centerline, located in the vertical symmetry plane at the Bellmouth exit or any other cross-section downstream from the Bellmouth exit is obtained using (7). Similarly, the yaw angle (Ψ) at any point on a line, normal to the centerline, located in the horizontal symmetry plane can be obtained using (8). The pitch (or yaw) flow angularity is defined using the maximum absolute pitch (or yaw) angle measured along this vertical (or horizontal) line. A plus or minus sign is added to these two maximum absolute angles depending on the axis convention employed here (Ref. (7) and (8)), where the X-axis coincides with the Bellmouth centerline and positive direction is oriented towards domain exit (Ref. Fig. 1 for the axis convention).

$$\theta = |tan^{-1}(\tfrac{v}{u})| \; and \; Pitch \; flow \; angularity = \pm \theta_{max} \quad (7)$$

$$\Psi = |tan^{-1}(\tfrac{w}{u})| \; and \; Yaw \; flow \; angularity = \pm \Psi_{max} \quad (8)$$

It is desirable to reduce the maximum pitch and yaw angles as much as possible at the honeycomb inlet with a proper Bellmouth intake design. The acceptability criterion set for the optimum Bellmouth design is that the magnitudes of both maximum flow angles measured on the respective symmetry planes at the honeycomb inlet must be less than 1°. A square cross-section (angle of rotational periodicity = 90°) means that magnitudes of maximum pitch and yaw angles are nearly the same, hence only pitch flow angularity is documented here.

The maximum wall pressure coefficient is defined as:

$$C_{pe} = 1 - \left(\frac{U_\infty}{V_e}\right)^2 \quad (9)$$

where the subscript 'e' refers to the point of maximum wall velocity just outside the boundary layer near the Bellmouth exit. The position of this maximum wall velocity is determined by plotting the static pressure distribution on the Bellmouth walls and identifying the minimum static pressure location in the contour plot. The maximum wall velocity is then obtained from the velocity profile plotted along a line drawn normal to the surface at the minimum static pressure location. It is worth noting here that the minimum static pressure is always located around the corner of the Bellmouth walls. In the case of nozzle contraction, Morel [60] showed that the magnitude of adverse pressure gradient around the nozzle exit is a function of C_{pe}. Hence, Morel employed C_{pe} to check the susceptibility of the turbulent boundary layer to separate in this adverse pressure gradient region. A maximum acceptable limit for C_{pe} was defined using the Stratford's separation criterion [61]. As C_{pe} was found to be linearly correlated with the nonuniformity at the Bellmouth exit ($\tilde{u}$), Morel [60] suggested that the maximum acceptability limit be placed on $\tilde{u}$ instead of C_{pe}. There is no separate acceptability criterion set for C_{pe} in the case of Bellmouth as well, as both $\tilde{u}$ and C_{pe} were found to be linearly correlated, Fig. 3. The $\tilde{u}$ and C_{pe} continues to follow the same linear positive correlation even with the addition of entry corner radius to the Bellmouth profile. The static pressure variation along the Bellmouth walls at the horizontal and vertical symmetry planes is also shown in Fig. 3. The static pressure reaches a local minimum near the exit but within the Bellmouth, resulting in an adverse pressure gradient downstream of this location.

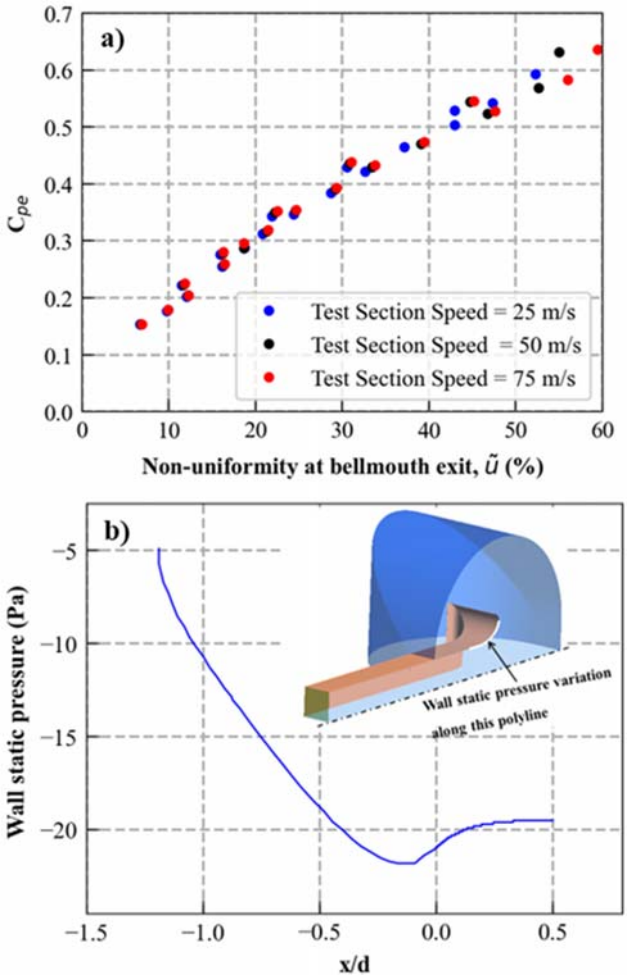

Fig. 3 (a) C_{pe} vs nonuniformity at Bellmouth exit $\tilde{u}$ for CR 9. (b) Static pressure variation along the Bellmouth walls at the vertical symmetry plane highlighted using white polyline: A portion of the constant area duct wall immediately after Bellmouth exit is also included in the polyline

The boundary layer growth along walls of Bellmouth and settling chamber increases the aerodynamic blockage due to an increase in the displacement thickness. The near-wall structured mesh is fine enough to resolve the viscous sublayer, as shown in Fig. 4. The boundary layer around the Bellmouth exit is already turbulent. A profile of the eddy viscosity ratio (a ratio of turbulent viscosity to molecular viscosity) shows a clear, sharp peak close to the wall (not shown here). When moving away from the wall, the eddy viscosity ratio transitions from a low value to a maximum value and then back to a low value inside the prism layers. As isotropic turbulence is assumed, the attached boundary layer thickness at any location can be predicted from the Reynolds stress profile [62], [63] at any location normal to the wall. The goal is to sufficiently reduce the boundary layer height with an optimized Bellmouth design

to decrease this aerodynamic blockage. The target is to reduce the non-dimensionless boundary layer thickness ($\frac{\delta}{d/2}$) at the honeycomb inlet below 5%. The performance parameters discussed above will be mapped with the corresponding geometrical parameters, and these will then be employed in evaluating different Bellmouth designs. The goal is to find a smallest-sized Bellmouth satisfying all four performance parameter specifications set earlier.

VI. Results and Discussions

Without Entry Corner Radius

A systematic parametric study was performed to find the optimum Bellmouth geometry for the IIT Tirupati wind tunnel. CFD simulations were carried out by varying the geometric (i.e., L/d and D/d) and kinematic (i.e., Re_d) parameters over a range of values decided based on previously reported studies in the literature [3], [4], [39]. The geometric parameters L/d and D/d were varied in steps of 0.2 from 0.3 to 0.9 and 1.3 to 1.9, respectively. Two different CR's 9 and 18, and three different test section flow speeds, 25 m/s, 50 m/s, and 75 m/s, were considered for this study. The test section dimensions together with the CR help establish the width of the square cross-sectional settling chamber, aiding in sizing the geometry at the Bellmouth exit. When multiple plots are shown in a figure in the result section, CR 9 and 18 are placed in the top and bottom rows, respectively. The identical markers in each plot are connected using piecewise linear trend lines.

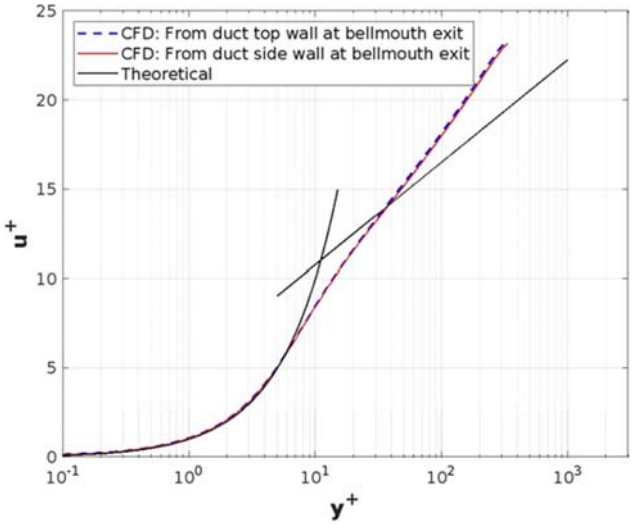

Fig. 4 Duct wall boundary layers, on the vertical and horizontal symmetry planes, at honeycomb inlet predicted by κ–ω SST model: Law of the wall is also shown in semi-logarithmic coordinates

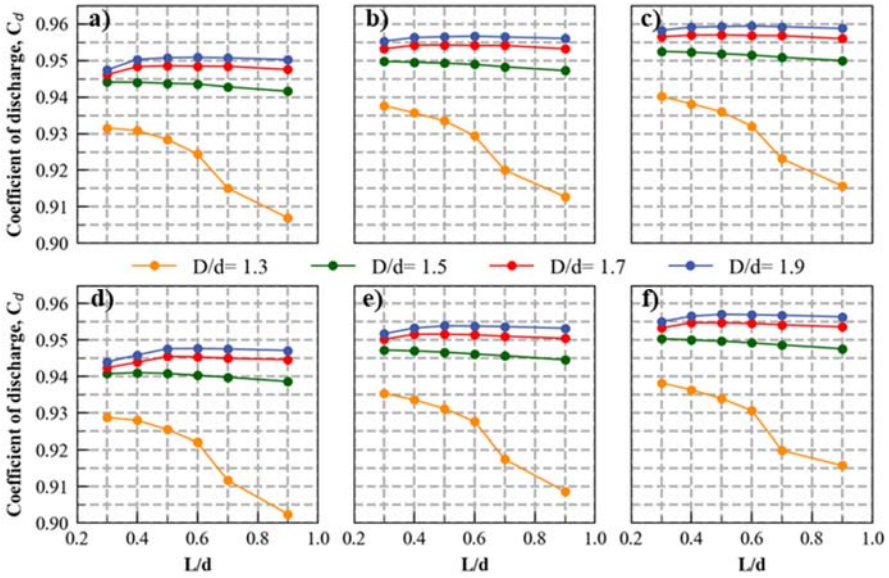

Fig. 5 Bellmouth design charts showing C_d variation with L/d for four different D/d values. Each plot in the top (or bottom) row is for a different test section speed, namely, 25 m/s (a), (d), 50 m/s (b), (e) and 75 m/s (c), (f). CR = 9 and CR = 18 are shown in the top and bottom rows, respectively

The efficiency of a Bellmouth is quantified in terms of the Coefficient of discharge (C_d). C_d is computed from (3), where the actual flow rate is calculated using the test section flow speed and is specified as an input in the CFD simulations at the domain outlet. Theoretical analysis is needed to compute the ideal flow rate. There is no total pressure loss between the domain inlet and domain outlet in ideal flow, assuming no recirculating regions around the domain outlet. The area-averaged static pressure at the domain outlet, obtained from each simulation, helps determine the "expected ideal flow rate" for the respective Bellmouth geometry.

Bellmouth design charts showing C_d variation with the geometrical parameters (L/d and D/d) at three different test section flow speeds and two different CR's are shown in Fig. 5. Each plot in the top (or bottom) row is for a different test section flow speed, namely, 25 m/s (a), (d), 50 m/s (b), (e) and 75 m/s

(c), (f). Similar trends are observed in all six plots presented in Fig. 5. In each plot, the lowest C_d values are obtained at D/d = 1.3 for any chosen L/d values. At D/d = 1.3, increase in L/d from 0.3 to 0.9 results in ~3% drop in the C_d values. This drop-in efficiency results from Bellmouth inlet flow separation occurring inside the domain (not shown here). A marked improvement in C_d of ~2% is obtained by moving from D/d = 1.3 to D/d = 1.5. At D/d = 1.5, C_d still shows a decreasing trend with L/d, but the rate of fall is much lower than those observed in the case of D/d = 1.3, and it appears as though C_d is independent of L/d. For all D/d values above 1.5, the C_d variation with L/d shows a distinct maximum inside the L/d range. The observed peak shifts toward larger L/d values when D/d is increased beyond 1.5. At a test section flow speed of 25 m/s, the Bellmouth efficiency drops by up to ~0.5% at these D/d values for L/d < 0.5.

In all six plots presented in Fig. 5, the maximum C_d at any L/d is obtained for D/d = 1.9. Nevertheless, the observed gain in C_d is relatively small ~0.2% when moving from D/d = 1.7 to D/d = 1.9. As observed in Fig. 5, for CR 9 and at test section flow speed of 25 m/s, only Bellmouth's belonging to a subset of the D/d = 1.9 family reaches a C_d value higher than 0.95. For CR 18, not a single Bellmouth geometry satisfies that criterion. The exit Reynolds number (Re_d) provides the necessary condition for dynamic similarity for a family of elliptical Bellmouth's whose geometry is defined using the two parameters L/d and D/d. The three different test section speeds and two different CRs also provide an opportunity to test the C_d dependency on exit Reynolds number (Re_d). There is a noticeable effect of exit Reynolds number (Re_d) on the resulting C_d values, as seen from the six plots in Fig. 5. The C_d values obtained for CR = 9 are always higher than the corresponding C_d values at CR = 18. The larger the Re_d, the greater the resulting C_d value, and this dependency is non-linear.

Bellmouth design charts will help design optimized Bellmouth's for low-speed wind tunnels as they serve as a set of universal curves providing practical value. Based on these plots, the initial impulsive reaction is to choose the largest D/d (i.e., 1.9 or even larger) for sizing a Bellmouth, as it produces the highest C_d values in all cases. We understandably want to choose a Bellmouth with as high efficiency as possible. However, the focus is on finding the smallest sized Bellmouth for our application, which costs less and occupies less space (remember, it will be housed inside a lab). Also, other performance parameters need to be evaluated and checked to understand their dependency on the geometrical parameters. Then the vital question to answer is: What minimum L/d and D/d will help satisfy all the four goals listed at the end of section 1?

The total pressure loss, ΔP_T, between domain inlet and domain outlet as a function of C_d for three different test section speeds and two CRs is shown in Fig. 6, where the ΔP_T is non-dimensionalized using the average dynamic pressure at domain exit. The CRs 9 and 18 are represented in Fig. 6 using a filled and cross marker, respectively. To start with, the total pressure losses in the Bellmouth are generally small as large CRs are employed here. The data obtained at various test section flow speeds from both CRs show a very good collapse along a straight line, whose equation can be obtained by linear regression using the method of least squares. The plot indicates that ΔP_T and C_d are negatively correlated but show a linear dependency following the relationship given in (10). At any CR, if the test section flow speed is doubled, say, from 25 m/s to 50 m/s then ΔP_T increases by a factor of four. Therefore, at large test section flow speeds, it is even more imperative to increase the Bellmouth efficiency as much as possible (i.e., maximize C_d) to keep the corresponding total pressure losses low. For $C_d > 0.95$, the total pressure losses in a Bellmouth are always less than 0.1.

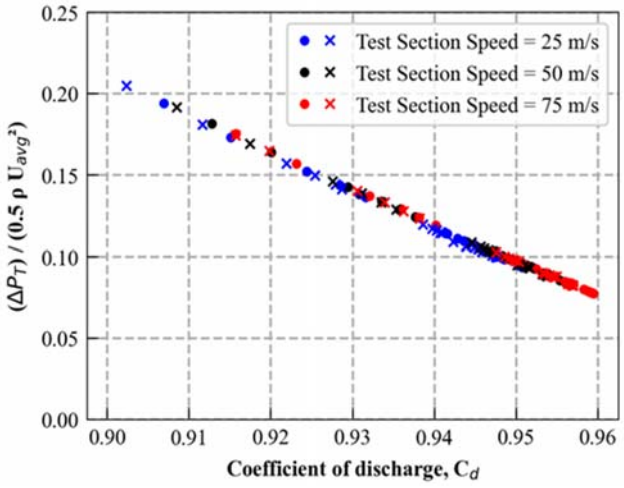

Fig. 6 Total pressure loss between domain inlet and domain outlet as a function of C_d for three different test section speeds (or Re_d), where the total pressure loss is non-dimensionalized using the average dynamic pressure at domain exit. CR's 9 and 18 (or Re_d) are shown using a filled circle and cross markers, respectively

$$\frac{\Delta P_T}{0.5\,\rho\,U_\infty{}^2} = -2.207 \times C_d + 2.193 \qquad (10)$$

The variation in pitch flow angularity at the Bellmouth exit as a function of the geometric parameter L/d for different D/d values is shown in Fig. 7 using solid lines, where its values can be read from the left-hand side y-axis. The flow angularity refers to the absolute maximum pitch angle (see (7)) measured on a vertical line located in the symmetry plane at Bellmouth exit. These absolute maximum pitch angles are negative because of the axis convention employed here, which signifies that the velocity vectors at Bellmouth exit are pointing downwards, resulting in a negative y-component. As the Bellmouth duct cross-sectional area is square, the magnitude of the absolute maximum yaw angle measured on a horizontal line in the symmetry plane at Bellmouth exit is around the same value, hence not shown. The nonuniformity as a function of the two geometric parameters is also shown in the same plot using dotted lines, and its values can be read from the y-axis located on the right-hand side. The nonuniformity at the Bellmouth exit plane is calculated using (6). All values shown in Fig. 7 are obtained at a test section flow speed of 50 m/s, but very similar

trends are seen at 25 m/s and 75 m/s. Again, CRs 9 and 18 are shown at the top and bottom plots, respectively. The identical markers are connected using piecewise linear trend lines to help identify their approximate variational behavior with L/d for different D/d values. For example, at D/d = 1.9 and L/d = 0.4, the maximum pitch angle is ~ -8.5 deg and nonuniformity is ~47% for CR = 9 and the corresponding values for CR=18 are ~ -10 deg and ~39%.

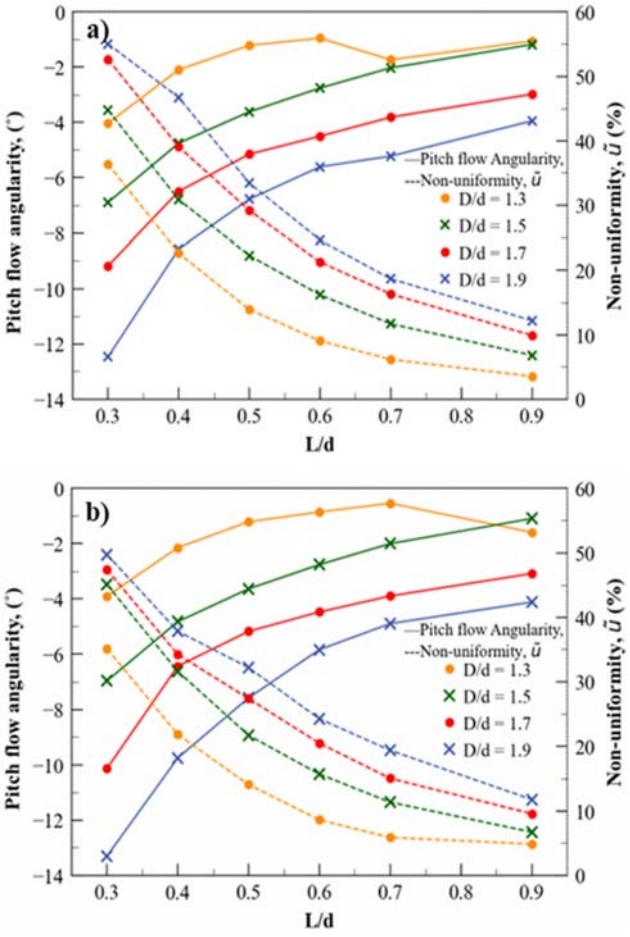

Fig. 7 Pitch flow angularity (solid line) and nonuniformity (dashed line) variation at Bellmouth exit with L/d for four different D/d values at a test section speed of 50 m/s. CRs 9 and 18 are shown at the (a), (b) plots, respectively

At any chosen L/d, the absolute flow angularity and nonuniformity are smallest for D/d = 1.3 and largest for D/d = 1.9 and vary nonlinearly with D/d. This is in direct contrast with the behavior of C_d observed in Fig. 5. Though shorter Bellmouth's (i.e., with small L/d values) may result in smaller boundary layer thickness at the Bellmouth exit, they have a significant impact on the two other performance parameters presented in Fig. 7. At any chosen D/d, the highest absolute flow angularity and nonuniformity values are observed in the shortest Bellmouth's, but they fall quickly with an increase in L/d values, as seen in Fig. 7. A large L/d is preferred at any D/d, as it produces a marked improvement in the absolute flow angularity and nonuniformity, resulting in a much better flow quality at the Bellmouth exit (and hence, also at honeycomb inlet). Therefore, it is better to choose a longer Bellmouth, but this is expected to increase the cost and exit boundary layer thickness. The boundary layer thickness at Bellmouth exit, as will be seen in Fig. 10, increases with an increase in L/d and D/d values. All these produce contradictory results emphasizing the need for tradeoffs in Bellmouth design for a low-speed wind tunnel.

The focus is on finding the smallest sized Bellmouth. From Figs. 5-7, it is possible to narrow down the design parameter range in which the final optimized Bellmouth geometry is expected to lie. The range of narrowed down L/d is from 0.5 to 0.6, and for D/d is from 1.5 to 1.7. It is observed that in all cases, the absolute flow angularity and nonuniformity at the Bellmouth exit reduces downstream along the flow direction. The evolution of flow angularity and nonuniformity downstream from Bellmouth exit is tracked for six different geometrical parameter pairs (i.e., L/d, D/d), namely, (0.3, 1.3), (0.3, 1.9), (0.9, 1.3), (0.9, 1.9), (0.5, 1.5), and (0.5, 1.7), shown in Fig. 8. Four of these pairs represent all possible combinations of the two extreme values for the geometrical parameter's L/d (= 0.3 and 0.9) and D/d (= 1.3 and 1.9). The other two pairs were chosen from the narrowed down range: (L/d, D/d) = (0.5, 1.5) and (L/d, D/d) = (0.5, 1.7), respectively. The identical markers in Fig. 8 are connected using piecewise linear trend lines to help better identify the different Bellmouth geometries.

As seen in Fig. 8, the nonuniformity evolution downstream from the Bellmouth exit plane shows an exponential decay for all cases reported in this manuscript, where 'x' is the distance downstream from the Bellmouth exit along the centerline (i.e., x-axis). A similar 'exponential decay' downstream of a wind tunnel contraction was observed and reported by Morel [60]. Five different x values in the range of 0 to 1 m in steps of 0.25 m are shown in Fig. 8, with x = 1.5 m also included for CR = 18. It is observed that the nonuniformity reaches a value of ~1% at x/d~0.48 from the Bellmouth exit and continues to decay further downstream. The flow angularity evolution downstream of Bellmouth exit is also shown in Fig. 8 using the left-hand side y-axis. The flow angularity is measured on a vertical line placed at different x/d locations in the vertical symmetry plane.

The absolute flow angularity also appears to decay faster in all cases, but to different values at x/d ~ 0.48, where almost all are above the target criteria of 1° set at honeycomb inlet. Increasing the D/d value at any L/d results in a larger absolute flow angularity and nonuniformity at the honeycomb inlet; hence larger D/d at any L/d must be avoided. But as seen in Fig. 5, the Bellmouth efficiency (i.e., C_d) increases with an increase in D/d values. Again, these produce conflicting results emphasizing the need for tradeoffs in Bellmouth design for a low-speed wind tunnel. This study is expected to yield the minimum distance from the Bellmouth exit at which a honeycomb must be located to minimize the total pressure loss and flow distortion across it.

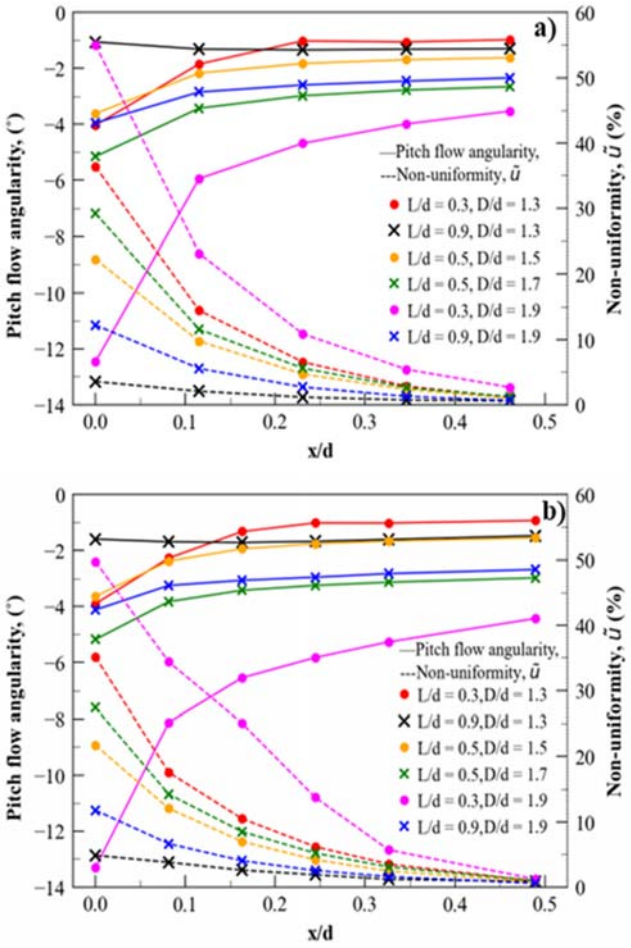

Fig. 8 Evolution of pitch flow angularity (solid line) and nonuniformity (dotted line) downstream from the Bellmouth exit for six different geometrical parameter pairs, where x is the centerline distance referenced from the Bellmouth exit. CRs 9 and 18 are shown in the (a), (b) plots, respectively

The difference between maximum and minimum static pressures at Bellmouth exit plane compared to nonuniformity (also obtained at Bellmouth exit plane) is shown in Fig. 9 for three different test section speeds (or Re_d): 25 m/s, 50 m/s, and 75 m/s. CRs = 9 and 18 are shown, respectively. The static pressure difference is non-dimensionalized using the average dynamic pressure at domain exit. As expected, both are positively correlated but there is also a good collapse of all data obtained at different test section speeds and CRs, showing a linear behavior. As seen in Fig. 9, a nonuniformity of 25% corresponds to a static pressure difference of 0.6 at the Bellmouth exit plane. A large nonuniformity correlates to a large static pressure difference at the Bellmouth exit plane, which in turn establishes a strong adverse pressure gradient downstream. This adverse pressure gradient accelerates boundary layer growth and creates a possibility for flow separation. Similarly, at any nonuniformity, the absolute static pressure difference is directly proportional to the square of average domain exit speed. This means that the established adverse pressure gradients are stronger at large test section speeds.

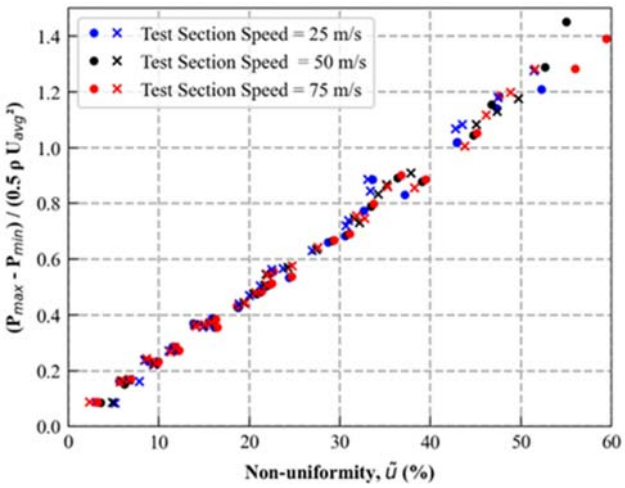

Fig. 9 The difference between maximum and minimum static pressures as a function of nonuniformity at Bellmouth exit plane for three test section speeds (or Re_d), where y-axis is non-dimensionalized using the average dynamic pressure at domain outlet. CRs 9 and 18 are shown using a filled circle and cross markers, respectively

The boundary layer thickness variation downstream of Bellmouth exit for the six different Bellmouth geometries is presented in Fig. 10. The boundary layer at the Bellmouth exit is already turbulent, and a turbulent kinetic energy profile at any desired location normal to the wall is employed to mark its edge. The boundary layer thickness variation on the vertical symmetry plane at different downstream distances from the Bellmouth exit for six different Bellmouth geometry is shown in Fig. 10. The y-axis is non-dimensionalized with d, and the identical markers are connected using piecewise linear trend lines. As noted in Fig. 5, C_d drops with an increase in L/d at D/d = 1.3 due to inlet flow separation at both CRs; this results in ~50% increase in the boundary layer thickness at Bellmouth exit. The boundary layer growth downstream from the Bellmouth exit is less in this case. At L/d = 0.3, an increase of D/d from 1.3 to 1.9 also results in a considerable increase in boundary layer height at Bellmouth exit and at honeycomb inlet. As expected, any increase in L/d or D/d results in a thicker boundary layer at the Bellmouth exit at both CRs. Finally, the boundary layer thickness at all downstream locations is slightly larger for CR 18 than with CR 9.

With Entry Corner Radius

Based on the above results, nine potential geometrical parameter pairs from the narrowed down range were chosen for further investigation. These potential candidate pairs are formed from all possible combinations of L/d = {0.5, 0.525, 0.55} and D/d = {0.1.625, 1.65, 1.675} subsets. According to [2], a substantial gain in performance can be realized by adding a quarter circle - with an entry corner radius (r) of 0.08 times the hydraulic diameter at Bellmouth inlet (D) - at the inlet of the elliptical profile. As a part of the study reported in this manuscript, three different entry corner radii (r/D) - 0.065, 0.08, and 0.095 - were independently tested with (L/d, D/d) = (0.5, 1.5) and (0.5, 1.7) (results not shown here), and it was found

that r/D = 0.095 produces a slightly improved performance compared to r/D = 0.08. At a test section speed of 50 m/s, the differences were less than ~-0.02% for C_d (i.e., C_d for r/D = 0.08 was larger), ~1% for nonuniformity as well as flow angularity, and ~0.01% in the case of boundary layer thickness. Nevertheless, the differences in performance parameters between r/D = 0.08 and r/D = 0.095 are negligibly small (possibly insignificant), but r/D = 0.08 results in a smaller-sized Bellmouth. Hence, it was decided to use r/D = 0.08 in the final design.

As seen in Fig. 11, the highest C_d values are recorded for the nine potential Bellmouth parameter pairs. These nine Bellmouth geometries show superior performance with C_d recording a jump of ~0.5% compared to the corresponding values at D/d = 1.7 (i.e., without entry corner radius) in all six plots. The highest Bellmouth efficiency recorded earlier (in Fig. 5) was for D/d = 1.9 without entry corner radius, but the efficiency of the nine newly chosen Bellmouth geometries is clearly above these highest values, thus emphasizing the importance of entry corner radius in a wind tunnel Bellmouth design. Still, other performance parameters also need to be checked before making the final decision. Also, as seen in Fig. 11, all the nine chosen candidate geometries satisfy the first performance criteria, as their C_d values are now above 0.95.

Flow angularity and nonuniformity at the Bellmouth exit for the nine chosen candidate geometries are plotted in Fig. 12. The flow angularity and nonuniformity are calculated using (7) and (6). A substantial improvement in flow angularity is obtained by introducing an entry corner radius in the Bellmouth design. The absolute flow angularity for all nine Bellmouth geometries reduces even below the corresponding values recorded for D/d = 1.5 without entry corner radius. The absolute flow angularity drops by more than 30% with the entry corner radius. However, the effect of entry corner radius on nonuniformity recorded at the Bellmouth exit plane is much less pronounced. The nonuniformity drops only by ~10% when entry corner radius is included in the Bellmouth design. At both CRs, the newly chosen Bellmouth geometries with an L/d of 0.55 produce the best performance, as seen in Fig. 12, where performance is quantified and benchmarked in terms of the lowest absolute flow angularity and nonuniformity at the Bellmouth exit. Also, D/d = 1.625 and 1.65 show better performance than D/d = 1.675 at both CR's. Both nonuniformity and absolute flow angle are least for L/d = 0.55 and D/d = 1.625. More can be learned by tracking their evolution downstream from the Bellmouth exit.

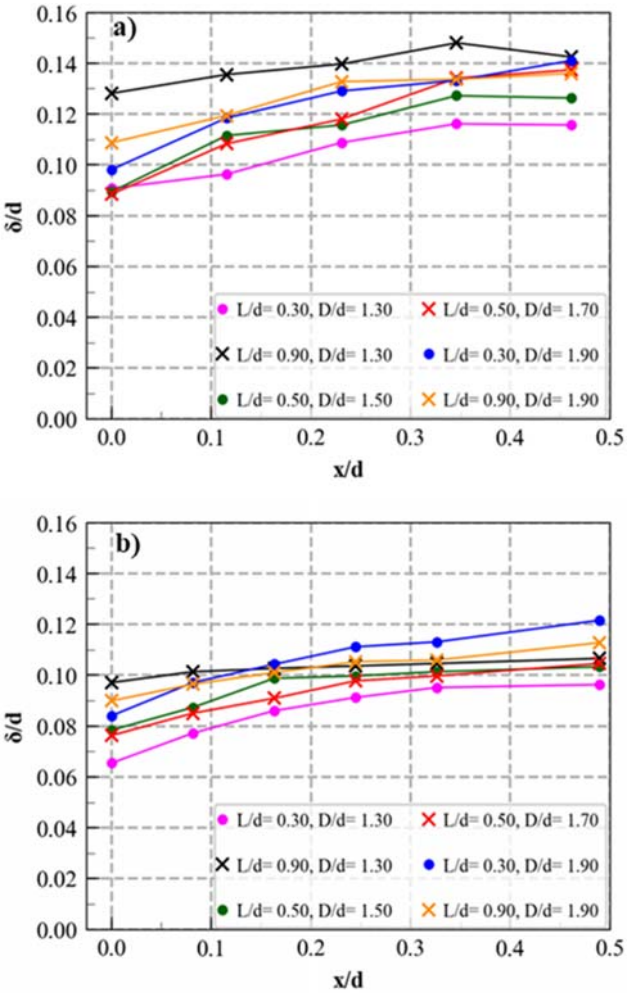

Fig. 10 Boundary layer thickness variation on the vertical symmetry plane at different downstream distances from the Bellmouth exit for six different Bellmouth geometry, where x is referenced from Bellmouth exit. CRs 9 and 18 are shown in the (a), (b) plots, respectively

Fig. 13 shows the evolution of pitch flow angularity and nonuniformity downstream from the Bellmouth exit for (L/d, D/d) = (0.55, 1.625) and (0.55, 1.65). Three other Bellmouth geometries are also included in the same plot: D/d = 1.65 (with entry corner radius), 1.5 (without entry corner radius), and 1.7 (without entry corner radius) all with L/d of 0.5. At both CRs, the absolute flow angularity drops faster when entry corner radius is provided to reach a value of ~0.3° at x/d ~ 0.47, which is about seven times smaller than the corresponding value obtained without entry corner radius. This satisfies the second criterion as the absolute maximum flow angles are now less than 1°. Similarly, nonuniformity shows an exponential drop in all five cases to reach a value of around 1% at x/d ~ 0.47. Honeycomb can be placed at this location. As we shall shortly see, the nonuniformity can be further reduced by a factor of three by switching from a square to a regular octagonal cross-sectional geometry.

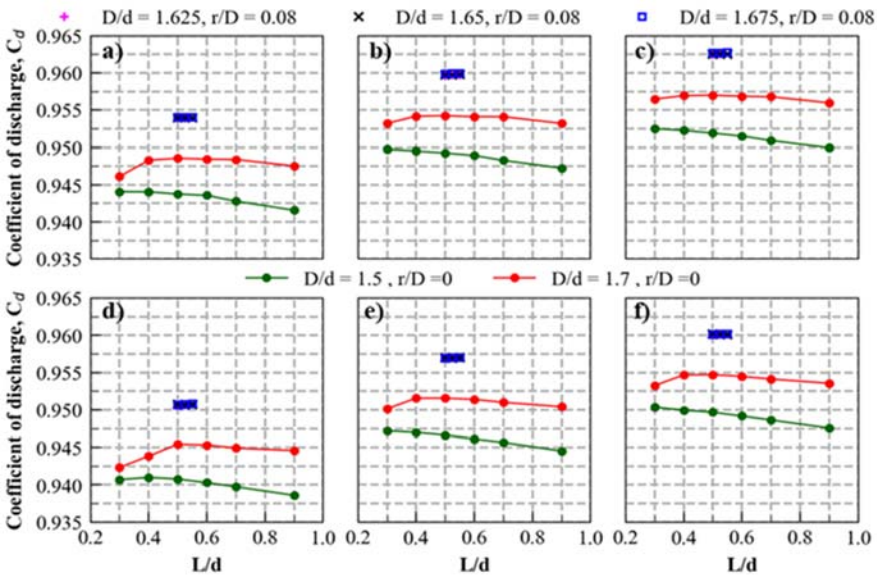

Fig. 11 C_d variation with L/d for nine chosen Bellmouth candidates with entry corner radius r/D = 0.08. D/d = 1.5 and 1.7 from design chars (in Fig. 5) also included for reference. Each plot in the top (or bottom) row represents CR 9 (or CR 18) with test section speeds of 25 m/s (a), (d), 50 m/s (b), (e) and 75 m/s (c), (f)

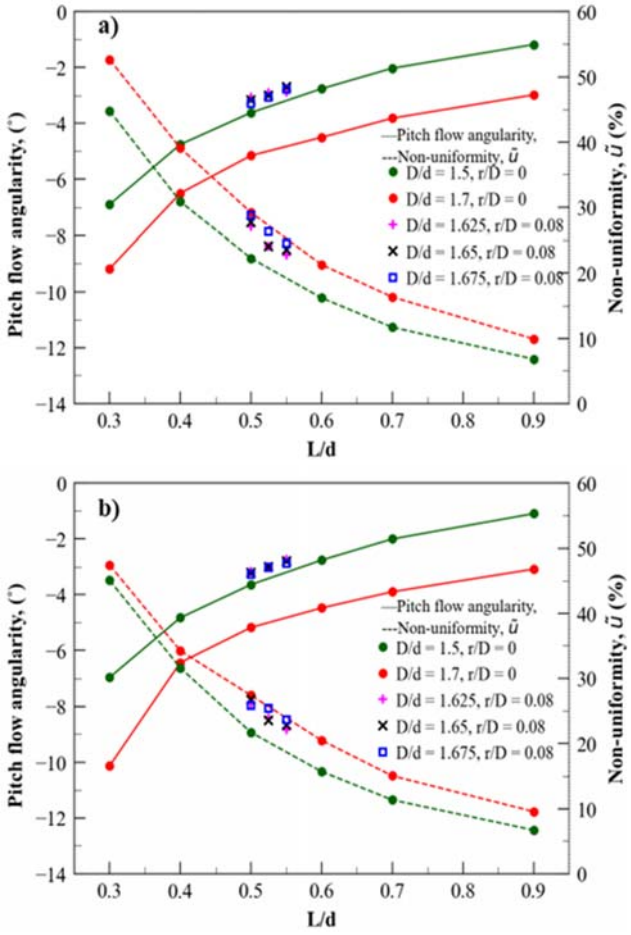

Fig. 12 Pitch flow angularity (solid line) and nonuniformity (dashed line) at the Bellmouth exit for the nine chosen geometry candidates with entry corner radius r/D = 0.08. D/d = 1.5 and 1.7 (Fig. 7) are also shown for reference. CR = 9 and CR = 18 are shown in (a), (b) respectively

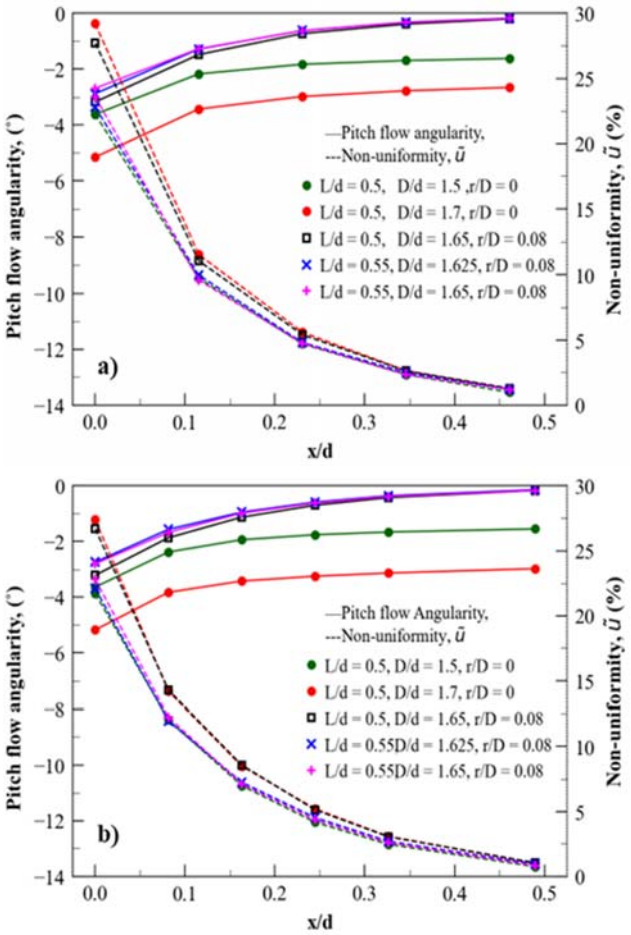

Fig. 13 Evolution of pitch flow angularity (solid line) and nonuniformity (dashed line) downstream from Bellmouth exit for five different geometries: three with entry corner radius and two without entry corner radius, where 'x' is referenced from Bellmouth exit. CR = 9 and CR = 18 are shown in (a), (b) respectively

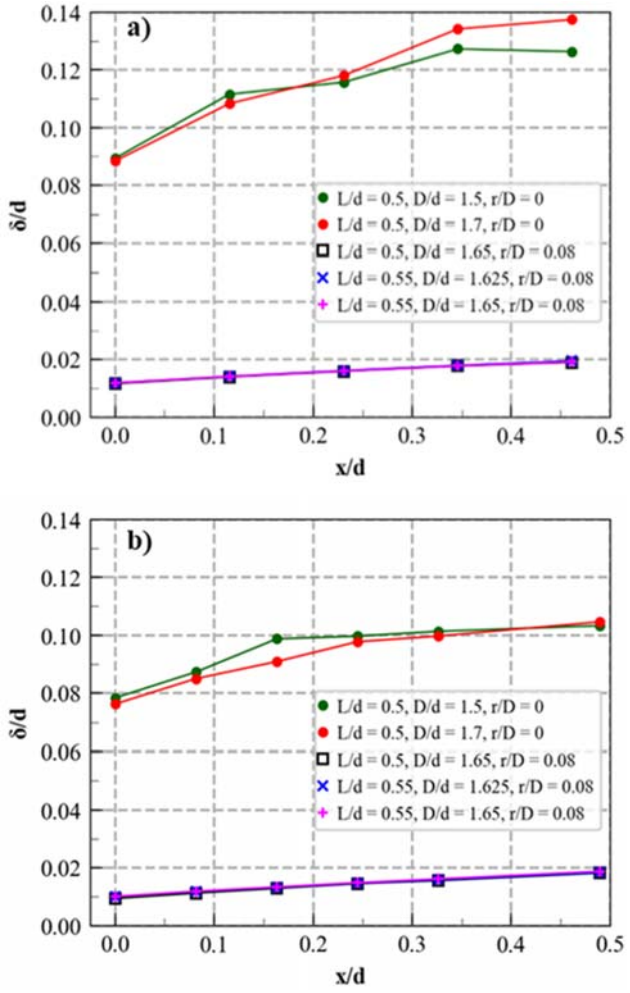

Fig. 14 Boundary layer thickness on the vertical symmetry plane as a function of downstream distance from the Bellmouth exit for five different Bellmouth configurations. CR = 9 and CR = 18 are shown in (a), (b) respectively

Finally, the boundary layer thickness evolution downstream from Bellmouth exit for configurations (L/d, D/d) = (0.55, 1.625) and D/d = (0.55, 1.65) with entry corner radius is shown in Fig. 14. Also included in the same plot for comparison are the configurations D/d = 1.65 (with entry corner radius), and D/d = 1.5, 1.7 (without entry corner radius), with an L/d of 0.5. At both CRs, the boundary layer thickness at the Bellmouth exit reduces by around one order of magnitude when the entry corner radius is added to the Bellmouth profile. The growth rate of the boundary layer downstream with the entry corner radius is also clearly lower. As seen in Fig. 14, the boundary layer thickness at all downstream locations increases with an increase in the CR. These plots clearly illustrate the benefits of adding an entry corner radius of r/D = 0.08 at the inlet of a Bellmouth profile. A small change in L/d or D/d with entry corner radius did not produce a perceptible change in the boundary layer thickness. The fourth performance criterion is now satisfied with the addition of entry corner radius to the Bellmouth profile as the non-dimensional boundary layer thickness ($\frac{\delta}{d/2}$) is now less than 5%.

The pitch flow angularity (solid line) and nonuniformity (dashed line) evolution downstream from the Bellmouth exit for two different Bellmouth geometries with regular octagonal cross-section is shown in Fig. 15 with an open circle marker. The two Bellmouth configurations with entry corner radius are D/d = 1.625 and 1.65, both having an L/d value of 0.55. The corresponding pitch flow angularity and nonuniformity values for a square cross-sectional geometry are also in the same plot for reference. Two different Bellmouth geometries without entry corner radii are also included for comparison in Fig. 15. All the values presented in Fig. 15 are for CR 9, but similar trends are observed with CR 18. When the Bellmouth duct cross-section is converted from a square to a regular octagon, surprisingly, there is a dramatic improvement in the flow nonuniformity both at the Bellmouth exit and at the honeycomb inlet. There is also a minor improvement in the pitch flow angularity. Other performance parameters do not change significantly. Both the Bellmouth and the settling chamber will have a regular octagonal cross-section. The nonuniformity at Bellmouth exit decreases from ~23% to ~14%, a ~40% drop is achieved by moving to a regular octagonal cross-section. Similarly, the nonuniformity at the honeycomb inlet reduces from ~1.25% to ~0.3%, ~four times fewer than the value recorded in the case of a square cross-section. It is possible to shorten the length of the settling chamber duct by employing a regular octagonal cross-section instead of a square, as the nonuniformity at x/d = 0.4 is already below the target level of 1%. The other three performance criteria are also satisfied at this location. Thus, the honeycomb can now be placed at a distance of x/d = 0.4 instead of x/d = 0.48 from the Bellmouth exit, a 20% reduction.

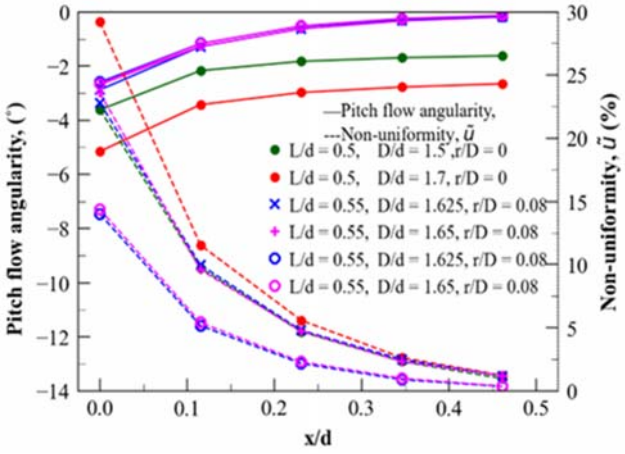

Fig. 15 Evolution of pitch flow angularity (solid line) and nonuniformity (dashed line) downstream from Bellmouth exit for regular octagon (open circle marker) vs. square (cross or plus marker) cross-section with entry corner radius for CR 9. (L/d, D/d) = (1.5, 1.7) without an entry corner radius is also shown

V. Conclusions

A systematic parametric study to identify the optimum Bellmouth profile for a low-speed open-circuit wind tunnel is reported. The optimized Bellmouth profile meets a certain set

of performance specifications and is found by mapping the performance parameters with the geometrical parameters. The essential takeaways are listed below.

1. Design charts for elliptically profiled Bellmouth's with two different CRs (9 and 18) and three different test section flow speeds (25 m/s, 50 m/s, 75 m/s) were presented. The range of geometrical parameters covered in this investigation includes 'L/d' from 0.3 to 0.9 and 'D/d' from 1.3 to 1.9.
2. Total pressure loss in the domain correlates negatively with C_d. There was an excellent collapse of all data collected at different CRs and test section flow speeds along a straight line, whose equation is documented. These kinds of relationships will be useful in actual measurements.
3. An entry corner radius of r/D = 0.08 added to the Bellmouth profile was found to reduce both the absolute flow angularity and boundary layer thickness at the honeycomb inlet (as well as at Bellmouth exit) while also improving the Bellmouth efficiency. The C_d jumps by ~0.5%, absolute flow angularity reduces by ~30%, and boundary layer thickness reduces by around seven times with an entry corner radius of r/D = 0.08.
4. Evolution of flow angularity, nonuniformity, and boundary layer thickness downstream from the Bellmouth exit up to x/d = 0.48 was presented for several Bellmouth geometries with and without entry corner radius.
5. P_{max}-P_{min} shows a positive linear correlation with nonuniformity at the Bellmouth exit, with a good collapse of data obtained at different CRs and test section speeds. These observations will be useful in actual measurements.
6. The nonuniformity at honeycomb inlet drops by around three times from ~1% to ~0.3% by changing the Bellmouth duct cross-sectional geometry from square to regular octagon.
7. A regular octagonal cross-section Bellmouth with dimensions of L/d = 0.55, D/d = 1.625 and r/D = 0.08 was selected for the final intake design. This design met all four performance specification criteria.
8. It is recommended that the honeycomb be placed at a minimum distance of x/d = 0.48 from the Bellmouth exit for a square cross-sectional Bellmouth geometry. But this can be reduced to x/d = 0.4 in the case of a regular octagonal cross-sectional geometry.
9. A variation in domain inlet turbulence intensities (1%, 2%, and 5%) and turbulence length scales (1 mm, 5 mm and 50 mm) had a negligibly small (< 0.1%) impact on the Bellmouth performance parameters.

REFERENCES

[1] Tiwari A., Patel S., Lad A., and Mistry C. S., "Development of Bell Mouth for Low Speed Axial Flow Compressor Testing Facility," *Proceedings of the Asian Congress on Gas Turbines, Indian Institute of Technology Bombay, India*, p. 14-16, 2016.

[2] Blair G. P., and Cahoon W. M., "Special Investigation: Design of an Intake Bellmouth," *Race Engine Technology 17*, p. 34-41, 2006

[3] Johl G., "The Design and Performance of a 1.9 mx 1.3 m Indraft Wind Tunnel," *Doctoral dissertation © Guru Johl*, 2010.

[4] Johl G., Passmore M., and Render P., "Design Methodology and Performance of an Indraft Wind Tunnel," *The Aeronautical Journal 108.1087*" p. 465-473, 2004.

[5] Barlow J. B., Rae Jr W. H., and Pope A., "Low Speed Wind Tunnel Testing," *John Wiley & Sons*, 1999.

[6] Mehta R. D., and Bradshaw P., "Design Rules for Small Low Speed Wind Tunnels," *The Aeronautical Journal 83.827*, p. 443-453, 1979.

[7] Bradshaw P., and Pankhurst R. C., "The Design of Low-Speed Wind Tunnels," *Progress in Aerospace Sciences 5*, p. 1-69, 1964.

[8] Barrett R. V., "Design and Performance of a New Low Turbulence Wind Tunnel at Bristol University," *The Aeronautical Journal 88.873*, p. 86-90, 1984.

[9] Cattafesta L., Bahr C., and Mathew J., "Fundamentals of Wind Tunnel Design," *Encyclopedia of Aerospace Engineering*, p. 1-10, 2010.

[10] Westphal R. V., "Wind Tunnel Design," *Thermal Measurements in Electronic Cooling*, CRC Press, p. 321-347, 2020.

[11] Hernández M. A. G., López A. I. M., Jarzabek A. A., Perales J. M. P., Wu Y., and Xiaoxiao S., "Design Methodology for a Quick and Low-cost Wind Tunnel," *Wind Tunnel Designs and their Diverse Engineering Applications*, p. 3-26, 2013.

[12] Mehta R. D., "Aspects of the Design and Performance of Blower Tunnel Components," *Doctoral dissertation, University of London*, 1979.

[13] Bradshaw P., "Experimental Fluid Mechanics," *The Commonwealth and International Library: Thermodynamics and Fluid Mechanics Division. Elsevier,* 2016.

[14] Celis B., and Ubbens H. H., "Design and Construction of an Open-Circuit Wind Tunnel with Specific Measurement Equipment for Cycling," *Procedia Engineering 147*, p. 98-103, 2016.

[15] Bell J. H., and Mehta R. D., "Contraction Design for Small Low-Speed Wind Tunnels," *No. NASA-CR-177488*, 1988.

[16] Morel T., "Comprehensive Design of Axisymmetric Wind Tunnel Contractions," *Journal of Fluid Engineering,* v. 97(2), p. 225-233, 1975.

[17] Morel T., "Design of Two-dimensional Wind Tunnel Contractions," *Journal of Fluid Engineering* v. 99(2), p. 371-377, 1977.

[18] Su Y., "Flow Analysis and Design of Three-Dimensional Wind Tunnel Contractions," *AIAA journal,* v. 29(11), p. 1912-1920, 1991.

[19] Mikhail M. N., "Optimum Design of Wind Tunnel Contractions," *AIAA Journal,* v. 17(5), p. 471-477, 1979.

[20] Zanoun E. S., "Flow Characteristics in Low-Speed Wind Tunnel Contractions: Simulation and Testing," *Alexandria Engineering Journal*, v. 57(4), p. 2265-2277, 2018.

[21] Ross J., Olson L., Meyn L., and Vanaken., J.O.H.A.N.N.E.SM., "A New Design Concept for Indraft Wind-Tunnel Inlets with Application to the National Full-Scale Aerodynamics Complex," *24th Aerospace Sciences Meeting*, 1986.

[22] Reneau L.R., Johnston J.P., and Kline S.J., "Performance and Design of Straight, Two-Dimensional Diffusers," *Journal of Basic Engineering,* v. 89(1), p. 141-150, 1967.

[23] Japiske D., "Turbomachinery Diffuser Design Technology," *Rolls Royce Internal Publication,* 1985.

[24] Klein A., "Effects of Inlet Conditions on Conical-Diffuser Performance," p. 250-257, 1981.

[25] ESDU 73024, "Performance of Conical Diffusers in Incompressible Flow,"

[26] Goldstein R., "Fluid Mechanics Measurements," 2017.

[27] McDonald A.T. and Fox R.W., "An Experimental Investigation of Incompressible Flow in Conical Diffusers," *International Journal of Mechanical Sciences 8.2,* p. 125-139, 1966.

[28] Wallis R.A., "Axial Flow Fans and Ducts," 1983.

[29] Loehrke R.I. and Nagib H.M., "Experiments on Management of Free-Stream Turbulence," *Illinois Inst Of Tech Chicago*, 1972.

[30] Teitel M., Dvorkin D., Haim Y., Tanny J. and Seginer I., "Comparison of Measured and Simulated Flow through Screens: Effects of Screen Inclination and Porosity," *Biosystems Engineering,* v. 104(3), p. 404-416, 2009.

[31] Middlestadt F., and J. Gerstmann., "Numerical Investigations on Fluid Flow through Metal Screens," 5th European Conference for Aeronautics and Space Sciences (EUCASS), Munich, Germany, 2014.

[32] Glatt E., Rief S., Wiegmann A., Knefel M. and Wegenke E., "Structure and Pressure Drop of Real and Virtual Metal Wire Meshes," *Fraunhofer ITWM,* v. 157, p. 56, 2009.

[33] Welsh A., "Low Turbulence Wind Tunnel Design and Wind Turbine Wake Characterization," *Master Thesis, University of Wisconsin-Milwaukee,* 2013.

[34] Groth J. and Johansson A.V., "Turbulence Reduction by Screens." *Journal of Fluid Mechanics,* v. 197, p. 139-155, 1988.

[35] Farell C. and Youssef S., "Experiments on Turbulence Management using

Screens and Honeycombs," *Journal of Fluids Engineering,* v. 118(1), p. 26-32, 1996.
[36] Fadilah P.A. and Erawan D.F., "Effect of Applying Screen and Honeycomb to the Flow Characteristic in Wind Tunnel based on CFD Simulation," *Journal of Physics: Conference Series. IOP Publishing*, v. 1130, No. 1, p. l012008, 2018.
[37] Ross J. C., "Theoretical and Experimental Study of Flow-Control Devices for Inlets of Indraft Wind Tunnels," *Doctoral dissertation, Iowa State University*, 1987.
[38] Kulkarni V., Sahoo N. and Chavan S.D., "Simulation of Honeycomb–Screen Combinations for Turbulence Management in a Subsonic Wind Tunnel," *Journal of Wind Engineering and Industrial Aerodynamics,* v. 99(1), p. 37-45, 2011.
[39] ESDU 80037, "Pressure Recovery of Axisymmetric Intakes at Subsonic Speeds."
[40] Massey B.S. and Ward-Smith J., *Mechanics of fluids. Crc Press*, 2018.
[41] Batill S.M., Caylor M.J. and Hoffman J.J., "An Experimental and Analytic Study of the Flow Subsonic Wind Tunnel Inlets," *Norte Dame Univ in Department of Aerospace and Mechanical Engineering*, 1983.
[42] Caldas L., Oertwig S., Rudolphi A., Meyer R., Enghardt L. and Tapken U., "Development and Assessment of an Inflow Control Device and a Bell-mouth for a Low-Speed Aeroacoustic Fan Rig," *25th AIAA/CEAS Aeroacoustics Conference*, p.2713, 2019.
[43] Mathew J., Bahr C., Carroll, B., Sheplak M. and Cattafesta L., "Design, Fabrication, and Characterization of an Anechoic Wind Tunnel Facility," *11th AIAA/CEAS Aeroacoustics Conference*, p. 3052, 2005.
[44] Kim S., Heo S., Cheong C. and Kim T.H., "Numerical and Experimental Investigation of the Bell-Mouth Inlet Design of a Centrifugal Fan for Higher Internal Flow Rate," *Journal of Mechanical Science and Technology,* v. 27.8, p. 2263-2273, 2013.
[45] Meher-Homji C.B. and Bromley A., "Gas Turbine Axial Compressor Fouling and Washing," *Proceedings of the 33rd Turbomachinery Symposium. Texas A&M University, Turbomachinery Laboratories*, 2004.
[46] Rajendran V.P. and Patel V.C., "Measurement of Vortices in Model Pump-Intake Bay by PIV," *Journal of Hydraulic Engineering,* v. 126(5), p. 322-334, 2000.
[47] Anwar H.O. and Amimilett M.B., "Vortices at Vertically Inverted Intake," *Journal of Hydraulic Research,* v. 18.2, p. 123-134, 1980.
[48] Townend H.C., "A Method of Air Flow Cinematography Capable of Quantitative Analysis," *Journal of the Aeronautical Sciences,* v. 3.10, p. 343-352, 1936.
[49] Luidens R.W., Stockman N.O. and Diedrich J.H., "An Approach to Optimum Subsonic Inlet Design," *American Society of Mechanical Engineers*, v. 79672, p. V01AT01A051, 1979.
[50] Stolarski T., Nakasone Y. and Yoshimoto S., "Engineering Analysis with ANSYS Software," *Butterworth-Heinemann*, 2018.
[51] Matsson J.E., "An Introduction to ANSYS Fluent 2021," *SDC Publications*, 2021.
[52] ANSYS, Inc., *ANSYS Fluent User's Guide, Release 20.1*, 2021.
[53] Menter F.R., "Two-equation Eddy-Viscosity Turbulence Models for Engineering Applications," *AIAA journal,* v. 32(8), p. 1598-1605, 1994.
[54] Zhang Y., Sun Z., van Zuijlen A. and van Bussel G., "Numerical Simulation of Transitional Flow on a Wind Turbine Airfoil with RANS-based Transition Model," *Journal of Turbulence,* v. 18(9), p. 879-898, 2017.
[55] Eleni D.C., Athanasios T.I. and Dionissios M.P., "Evaluation of the Turbulence Models for the Simulation of the Flow over a National Advisory Committee for Aeronautics (NACA) 0012 Airfoil," *Journal of Mechanical Engineering Research,* v. 4(3), p. 100-111, 2012.
[56] Blazek J., "Computational Fluid Dynamics: Principles and Applications. Butterworth-Heinemann," 2015.
[57] Speziale C.G., "On Turbulent Secondary Flows in Pipes of Noncircular Cross-Section," *International Journal of Engineering Science,* v. 20(7), p. 863-872, 1982.
[58] White F.M., "Fluid mechanics," *Tata McGraw-Hill Education*, 1979.
[59] Holman J.P., "Experimental Methods for Engineers," 2012.
[60] Morel T., "Comprehensive Design of Axisymmetric Wind Tunnel Contractions," p. 225-233, 1975.
[61] Stratford B.S., "The Prediction of Separation of the Turbulent Boundary Layer." *Journal of fluid mechanics,* v. 5(1), p. 1-16, 1959.
[62] Cousteix J., "Aircraft Aerodynamic Boundary Layers," *Encyclopedia of Physical Science and Technology (Third Edition),* p. 301-317, 2003.
[63] Flierl G., and Ferrari R., "Turbulence in the Ocean and Atmosphere," *Massachusetts Institute of Technology: MIT OpenCourseWare, https://ocw.mit.edu/. License: Creative Commons BY-NC-SA*, 2007.